Signal Design and Detection in Presence of Nonlinear Phase Noise

Alan Pak Tao Lau, *Student Member, IEEE*, and Joseph M. Kahn, *Fellow, IEEE*

***Abstract*—In optical fiber transmission systems using inline amplifiers, the interaction of a signal and amplifier noise through the Kerr effect leads to nonlinear phase noise that can impair the detection of phase-modulated signals. We present analytical expressions for the maximum-likelihood (ML) decision boundaries and symbol-error rate (SER) for phase-shift keying and differential phase-shift keying systems with coherent and differentially coherent detection, respectively. The ML decision boundaries are in the form $\theta(r) = c_2 r^2 + c_1 r + c_0$, where θ and r are the phase and the amplitude of the received signal, respectively. Using the expressions for the SER, we show that the impact of phase error from carrier synchronization is small, particularly for transoceanic links. For modulation formats such as 16-quadrature amplitude modulation, we propose various transmitter and receiver phase rotation strategies such that the ML detection is well approximated by using straight-line decision boundaries. The problem of signal constellation design for optimal SER performance is also studied for a system with four signal points.**

***Index Terms*—Maximum likelihood (ML) detection, nonlinear optics, optical fiber communication, optical Kerr effect, phase noise, quadrature amplitude modulation (QAM).**

I. Introduction

OPTICAL fiber transmission systems using coherent or differentially coherent detection of phase-modulated signals, such as phase-shift keying (PSK), differential phase-shift keying (DPSK), or quadrature amplitude modulation (QAM), are subject to impairment by phase noise as well as amplitude noise. Amplified spontaneous emission (ASE) from inline amplifiers is a major source of noise and is referred to as *linear noise* in this paper. Gordon and Mollenauer [1] showed that signal and ASE can interact via the fiber Kerr nonlinearity to produce *nonlinear phase noise* (NLPN). Since NLPN is a major system impairment, particularly for long haul links [2]–[4], methods to mitigate the effect of NLPN and/or system designs in the presence of NLPN are required. The impact of fiber nonlinearities on system performance has been investigated since the 1990s [5], [6]. Various approaches have been studied to mitigate the effect of nonlinearities, such as path-averaged signal power minimization [7] or phase noise variance minimization [8]–[10], by designing the gains and spacings of the inline amplifiers. Management of dispersion and signal power [11], [12] and inline phase-noise compensation techniques such as placement of phase modulators along the fiber link [13] have also been considered. Furthermore, receiver-based detection or compensation techniques that exploit the correlation between received power and phase [14]–[16] have been proposed. However, few studies have been undertaken to investigate signal design and maximum-likelihood (ML) detection in systems with nonlinearity. In this paper, we focus on single-channel systems, neglecting chromatic dispersion and multichannel effects and considering self-phase modulation-induced NLPN only. We study signal design and implementation of ML detection for phase-modulated systems with linear phase noise and NLPN. For PSK/DPSK systems, we present analytical derivations for the ML decision boundaries and show how to approximate ML detection by phase postcompensation and straight-line decision boundaries. For 16-QAM systems, we propose signal design strategies such that ML detection can be well approximated by using straight-line decision boundaries. We also obtain analytical expressions for the system symbol-error rate (SER).

Our paper is organized as follows. In Section II, we study the PSK and DPSK systems with coherent or differentially coherent detection and derive analytical expressions for the ML decision boundaries and the corresponding SERs. We evaluate the impact of the phase error from carrier synchronization on SER performance, and we show that it is negligible, particularly for transoceanic links. In Section III, we focus on 16-QAM systems. For different degrees of system nonlinearity, we study various phase rotation techniques at the transmitter and the receiver such that ML detection is well approximated by using straight-line decision boundaries. Finally, in Section IV, we investigate the problem of signal constellation design to optimize SER performance for a system with four signal points.

II. ML Detection for PSK/DPSK Systems

In this section, we study PSK and DPSK systems with coherent or differentially coherent detection, respectively. As the signal power is the only design parameter and its effects on system performance have been studied elsewhere in the literature, we will focus on the implementation of ML detection in these systems. We will analytically derive the ML decision boundaries and the corresponding SERs.

Consider a transmission system of length L. For analytical convenience, we assume that the system uses distributed

Manuscript received March 18, 2007; revised July 3, 2007. This work was supported by the Defense Advanced Research Project Agency under the TACOTA Program under Prime Contract W911-QX-06-C-0101 via a subcontract from CeLight, Inc. Part of this work was presented at the LEOS Summer Topicals, Portland, OR, July 2007.

The authors are with the Department of Electrical Engineering, Stanford University, Stanford, CA 94305 USA (e-mail: alanlau@stanford.edu; jmk@ee.stanford.edu).

Color versions of one or more of the figures in this paper are available online at http://ieeexplore.ieee.org.

Digital Object Identifier 10.1109/JLT.2007.905217

TABLE I
PARAMETER VALUES USED IN THIS PAPER

γ	1.2 W^{-1}/km	α	0.25 dB/km
$\Delta\nu_{opt}$	42.7 GHz	n_{sp}	1.41
$\lambda = c/\nu$	1.55 μm		

amplification, where the incremental amplifier gain compensates for the incremental fiber loss. We assume that dispersion and multichannel effects are negligible. The ASE noise generated by the inline amplifiers accumulates at the receiver and is generally modeled as complex zero-mean circularly symmetric Gaussian random variables with variance in two polarizations

$$\sigma^2 = 2S_{sp}\Delta\nu_{opt} = 2h\nu n_{sp}\Delta\nu_{opt}\alpha L = b\alpha L \tag{1}$$

where $\Delta\nu_{opt}$ is the bandwidth of an optical filter at the receiver, n_{sp} is the spontaneous emission factor, ν is the signal frequency, and α is the attenuation coefficient. We will model a system using nonreturn-to-zero (NRZ) pulses operating at 42.7 GSymbol/s (40 GSymbol/s with 7% forward error correction overhead) throughout the paper. The bit rate is 80 Gb/s for quaternary signals and 160 Gb/s for 16-QAM signals.

As for the received signal, let the received phase be θ and define the received amplitude r as the received electric field amplitude divided by σ. For an NRZ signal with input power P and phase θ_o, the joint probability density function (pdf) of the received amplitude and phase is given by [2]

$$f_{P,\theta_o}(r,\theta) = \frac{f_R(r,P)}{2\pi} + \frac{1}{\pi}\sum_{m=1}^{\infty}\mathbf{Re}\left\{C_m(r)e^{jm(\theta-\theta_o)}\right\} \tag{2}$$

where

$$f_R(r,P) = 2re^{-(r^2+P/\sigma^2)}I_0(2r\sqrt{P/\sigma^2})$$

is the Rice pdf of the received amplitude, $\rho_s = P/\sigma^2$ is the optical signal-to-noise ratio (OSNR), and $\mathbf{Re}\{\cdot\}$ denotes the real part of a complex number. The Fourier coefficient $C_m(r)$ is given by

$$C_m(r) = \frac{r\sec\sqrt{jmx}}{s_m}e^{\rho_s\sqrt{jmx}\tan\sqrt{jmx}}e^{-\frac{r^2+\alpha_m^2}{2s_m}}I_m\left(\frac{\alpha_m r}{s_m}\right) \tag{3}$$

where

$$x = \frac{\gamma PL}{\rho_s + 1/2}, \quad \alpha_m = \sqrt{\rho_s}\sec\sqrt{jmx}, \quad s_m = \frac{\tan\sqrt{jmx}}{2\sqrt{jmx}}$$

and $I_m(\cdot)$ denotes the mth-order modified Bessel function of the first kind. Table I lists the parameter values used in this paper.

As an illustration, the received signal pdf and decision boundaries for a 4-PSK system are shown in Fig. 1 for an input power of -4 dBm after $L = 5000$ km of signal propagation. The pdf is distorted from the circular Gaussian shape, and the ML decision boundaries are spiral-like, indicating the presence of NLPN.

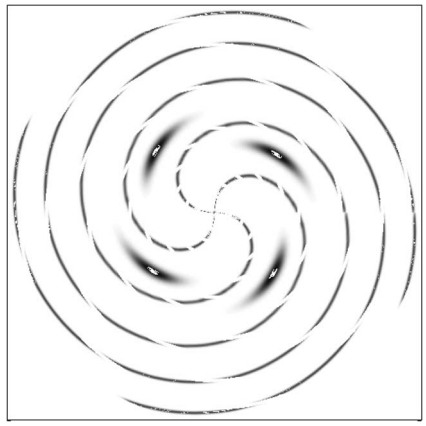

Fig. 1. Received signal pdf and corresponding ML decision boundaries (shown as dashed lines) for a 4-PSK system in presence of nonlinear phase noise. The signal power is -4 dBm, and the system length is 5000 km.

A. ML Decision Boundaries

To implement ML detection, we would need to know the ML decision boundaries as a function of ρ_s, θ_o, r, and θ. With knowledge of the boundaries, we can either implement a 2-D lookup table (such as the one proposed by [14]) that maps the received signal to one of the signal points or compensate the phase of the received signal and implement straight-line decision boundaries. As the two methods are equivalent to each other, we will focus on the latter and refer to it as *phase postcompensation* for the rest of this paper.

For an M-PSK system with rate $R = \log_2 M$ b/symbol, without loss of generality, we can focus our attention on one of the transmitted signal points s_o with power P, phase $\theta_o = 0$, and corresponding received pdf $f_{P,0}(r,\theta)$. Define the center phase $\theta_c(r)$ of $f_{P,0}(r,\theta)$ such that $[\theta_c(r) - \pi/M, \theta_c(r) + \pi/M]$, $r \in \mathbb{R}$, denotes the region where the received signal is mapped to s_o under ML detection. In this case, the optimal phase postcompensation operation can be mathematically defined as

$$\theta' = \theta - \theta_c(r)$$

where θ' is the signal phase after compensation, and the corresponding ML decision boundaries will be at $\theta' = \pm\pi/M$. The center phase $\theta_c(r)$ satisfies the relation

$$f_{\rho_s,0}(r,\theta_c + \pi/M) = f_{\rho_s,0}(r,\theta_c - \pi/M). \tag{4}$$

In the Appendix, it can be shown that with some approximations

$$\theta_c(r) = \sqrt{\frac{x}{2}}\frac{\sin\sqrt{2x} - \sinh\sqrt{2x}}{\cosh\sqrt{2x} - \cos\sqrt{2x}}r^2 - 4\sqrt{\frac{\rho_s x}{2}}\frac{\sin\sqrt{\frac{x}{2}}\cosh\sqrt{\frac{x}{2}} - \cos\sqrt{\frac{x}{2}}\sinh\sqrt{\frac{x}{2}}}{\cosh\sqrt{2x} - \cos\sqrt{2x}}r + h(x,\rho_s) \tag{5}$$

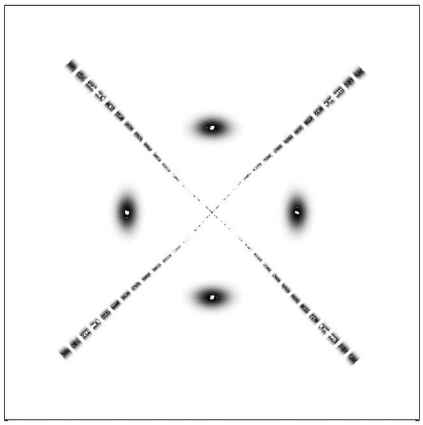

Fig. 2. Received signal pdf and corresponding ML decision boundaries (shown as dashed lines) after optimal phase post-compensation for a 4-PSK system. The signal power is -4 dBm, and the system length is 5000 km. The resulting decision boundaries are straight lines, allowing easy implementation of ML detection.

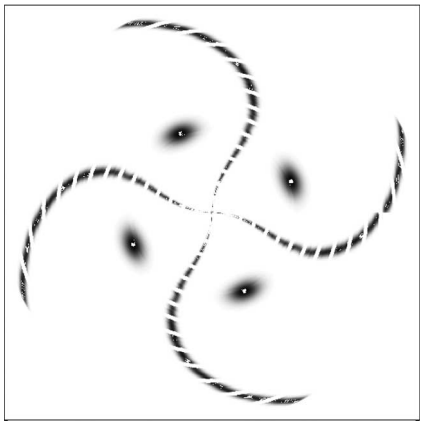

Fig. 3. Received signal pdf and corresponding ML decision boundaries (shown as dashed lines) after phase rotation using Ho and Kahn's [14] method for a 4-PSK system. The signal power is -4 dBm, and the system length is 5000 km.

where $h(x,\rho_s)$ is a function independent of r defined in the Appendix. Notice that $\theta_c(r)$ is in the form $c_2r^2+c_1r+c_0$, which is in contrast to the form $\sum_{i=1} c_{2i}r^{2i}$ that is used in some experiments [4], [16] for NLPN mitigation or other forms suggested by Ho [2] for phase noise variance minimization. In addition, $\theta_c(r)$ is independent of M. If we rotate the received signal by $\theta_c(r)$, the resulting decision boundaries are shown in Fig. 2. The straightness of the decision boundaries validates the approximations used in the derivation of $\theta_c(r)$ and shows that one can implement ML detection simply by rotating the received phase by $\theta_c(r)$. As a comparison, Fig. 3 shows the resulting decision boundaries after received phase rotation using Ho and Kahn's [14] method. The performance obtained using straight-line decision boundaries with that method will be inferior to that of ML detection.

B. SER for M-PSK and M-DPSK Systems

Using the analytical expression for the center phase $\theta_c(r)$, we can approximately implement ML coherent detection in M-PSK systems by optimal phase postcompensation and straight-line decision boundaries. In addition, we can also analytically derive the system performance measured in terms of the SER. Let the phase after phase postcompensation be $\theta'=\theta-\theta_c(r)$. The SER using straight-line decision boundaries is then given by

$$\begin{aligned}
&1-P(\text{correct detection})\\
&=1-\int_0^{\infty}\int_{-\pi/M}^{\pi/M} f_{P,0}\left(r,\theta'+\theta_c(r)\right)d\theta' dr\\
&=\frac{M-1}{M}-\frac{1}{\pi}\int_0^{\infty}\int_{-\pi/M}^{\pi/M}\sum_{m=1}^{\infty}\mathbf{Re}\Big\{C_m(r)e^{jm(\theta'+\theta_c(r))}\Big\}d\theta' dr\\
&=\frac{M-1}{M}-\sum_{m=1}^{\infty}\frac{2}{M}\mathrm{sinc}\Big(\frac{m\pi}{M}\Big)\int_0^{\infty}\mathbf{Re}\Big\{C_m(r)e^{jm\theta_c(r)}\Big\}dr\\
&=\frac{M-1}{M}-\sum_{m=1}^{\infty}\frac{2}{M}\mathrm{sinc}\Big(\frac{m\pi}{M}\Big)\int_0^{\infty}|C_m(r)|dr. \qquad (6)
\end{aligned}$$

In the Appendix, it is shown that the SER can be expressed as

$$\begin{aligned}
\text{SER}=&\frac{M-1}{M}-\sum_{m=1}^{\infty}\frac{2}{M}\,\mathrm{sinc}\left(\frac{m\pi}{M}\right)\\
&\times\mathbf{Re}\Bigg\{u_m(x)\times\sum_{k=0}^{\infty}\frac{\left(jg_m(x)\right)^k}{k!}\\
&\times\frac{\beta_m(x)^m\Gamma\left(\frac{m+k+2}{2}\right)}{2^{m+1}a_m(x)^{\frac{m+k+2}{2}}\Gamma(m+1)}\\
&\times{}_1F_1\left(\frac{m+k+2}{2},m+1;\frac{\beta_m^2(x)}{4a_m(x)}\right)\Bigg\} \qquad (7)
\end{aligned}$$

where ${}_1F_1(p,q;z)$ is the confluent hypergeometric function of the first kind, $\Gamma(z)$ is the Gamma function, and $a_m(x),\beta_m(x),g_m(x),$ and $u_m(x)$ are functions of m and x, which are defined in the Appendix.

In addition, the marginal pdf of the phase after optimal phase postcompensation θ' will be given by

$$\begin{aligned}
f(\theta')&=\int_0^{\infty} f_{P,0}\left(r,\theta'+\theta_c(r)\right)dr\\
&=\frac{1}{2\pi}+\frac{1}{\pi}\sum_{m=1}^{\infty}\left(\int_0^{\infty}|C_m(r)|\,dr\right)\cos(m\theta').
\end{aligned}$$

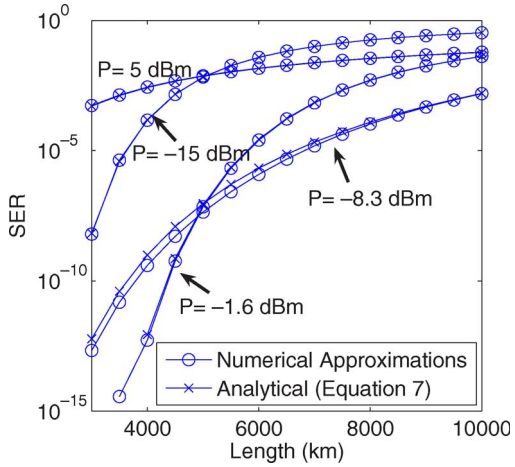

Fig. 4. SER for a 4-PSK system with coherent detection for various input power levels and system lengths. ML detection is used.

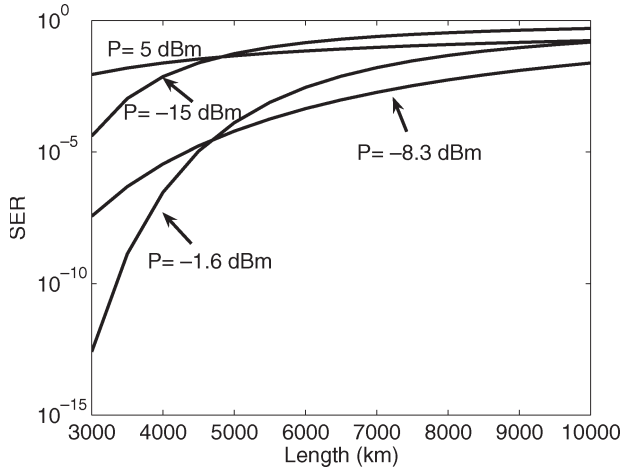

Fig. 5. SER for a 4-DPSK system with differentially coherent detection for various input power levels and system lengths. ML detection is used.

For M-DPSK systems with differentially coherent detection, the differential phase θ_d between a symbol and the previous symbol will have a pdf

$$f_d(\theta_d) = \frac{1}{2\pi} + \frac{1}{\pi}\sum_{m=1}^{\infty}\left(\int_0^{\infty}|C_m(r)|\,dr\right)^2\cos(m\theta_d). \quad (8)$$

Similar to the SER of M-PSK systems, it can be shown that the SER of M-DPSK systems is given by

$$\text{SER}_d = \frac{M-1}{M} - \sum_{m=1}^{\infty}\frac{2}{M}\,\text{sinc}\left(\frac{m\pi}{M}\right)\left(\int_0^{\infty}|C_m(r)|\,dr\right)^2. \quad (9)$$

The SER of a 4-PSK system as a function of L is shown in Fig. 4 for various input power levels. We can see that the analytical expression of (7) generally agrees well with numerical results [obtained by numerically integrating $f_{\rho_s}, 0(r,\theta)$ over the region that corresponds to ML detection error on the signal constellation plane]. The noise power and, hence, the SER increase with system length, and for each L, there exists an optimal input power that minimizes the SER. The SER for a 4-DPSK system is shown in Fig. 5. Compared with that of a 4-PSK system, the SER is generally larger in a 4-DPSK system for the same input power level and L and exhibits similar trends. These results are in agreement with expectations.

Using (6), it is also possible to study the system impact of other impairments, such as phase error resulting from carrier synchronization. Let the distribution of this phase error be

$$f_{err}(\theta) = \sum_{m=0}^{\infty}\mathbf{Re}\left\{D_m e^{jm\theta}\right\}. \quad (10)$$

As the phase error directly adds to the received phase, the pdf of the overall received phase f_{overall} is the convolution of f_R, θ_o with f_{err}. When f_{overall} is expressed as a summation of Fourier components, the mth Fourier coefficient is simply given by $D_m C_m(r)$. The phase error should be symmetric about 0, and hence, D_m is a real number and does not affect the derivation of the ML decision boundaries (see the Appendix). However, the SER performance is expected to worsen with increasing phase errors from carrier synchronization. To numerically illustrate its impact, we consider a digital feedforward carrier recovery system (such as the one studied by Ip and Kahn [17]) in which the phase error is known to be Gaussian distributed. Fig. 6 shows the SER of a 4-PSK system as a function of L and the standard deviation of the phase error. From the figure, the impact of phase errors is more profound when the SER is low, and the impact is small for transoceanic links with length typically over 5000 km.

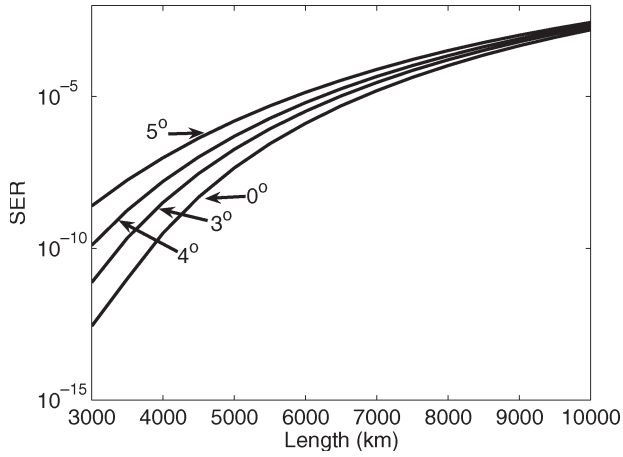

Fig. 6. SER for a 4-PSK system using ML detection with phase error from carrier synchronization. The power of the signal is −8 dBm, and the degree values represent the standard deviation of the phase error.

III. QAM Signal Design and ML Detection Strategies

In this section, we focus on signaling schemes encoding over 2 b/symbol, such as 16-QAM with coherent detection. We separately study systems with low and high nonlinearities and propose various phase rotation techniques at the transmitter and receiver to approximate ML detection using straight-line decision boundaries.

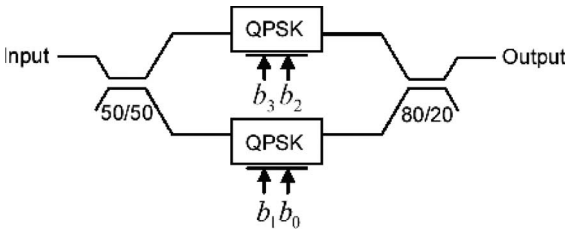

Fig. 7. A 16-QAM transmitter setup. A continuous wave input is equally split into two branches and passed through two QPSK modulators modulated by bit streams b_0, b_1, b_2, and b_3. The outputs are then combined with unequal weights, resulting in a 16-QAM signal set.

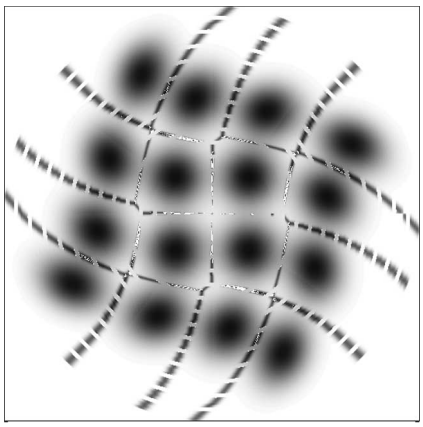

Fig. 8. Received signal pdf and corresponding ML decision boundaries (shown as dashed lines) for a square 16-QAM system with $P_{avg} = -13$ dBm and $L = 3000$ km.

A. Low Nonlinearity Regime

We will start with a usual square 16-QAM constellation with points located at

$$\sqrt{P}e^{j\left(\pm\frac{\pi}{4}\pm\pi\right)}, \qquad \sqrt{9P}e^{j\left(\pm\frac{\pi}{4}\pm\pi\right)}$$
$$\sqrt{5P}e^{j\left(\pm\tan^{-1}(1/3)\pm\frac{\pi}{2}\right)}, \qquad \sqrt{5P}e^{j\left(\pm\tan^{-1}(3)\pm\frac{\pi}{2}\right)}$$

and average power $P_{avg} = 5P$. A 16-QAM transmitter setup is shown in Fig. 7. The received pdf and the corresponding ML decision boundaries are shown in Fig. 8 for a system with $P_{avg} = -13$ dBm and $L = 3000$ km.

With this constellation set, we cannot perform optimal phase postcompensation, as the transmitted power is not constant for all the signals, whereas evaluating $\theta_c(r)$ given by (5) depends on the knowledge of the transmitted power. However, for 16-QAM systems with low degree of nonlinearity, the decision boundaries (such as those shown in Fig. 8) are close to straight lines, and it may be possible to design the transmitted signal set or process the received signal such that the ML detection boundaries are well approximated by straight lines. As a first step, we can prerotate each of the 16 signal points by its mean nonlinear phase shift $\overline{\theta_{NL}}$ such that the modes of the conditional pdfs coincide with those in a linear 16-QAM system. This will be referred to as phase precompensation, and one such example is shown in Fig. 9 for $P_{avg} = -1$ dBm. As NLPN is a major limiting factor in system performance, techniques

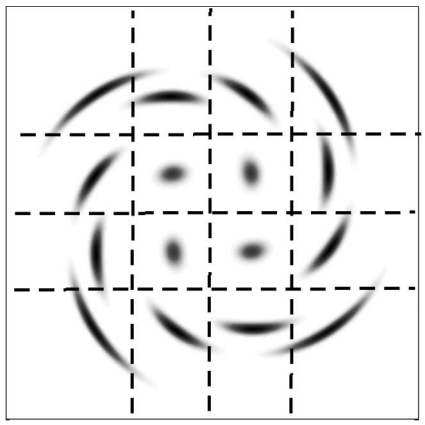

Fig. 9. Received signal pdf for a 16-QAM system with phase precompensation only. (Dashed lines) Straight-line decision boundaries used for detection. The average power is -1 dBm, and the system length is 3000 km.

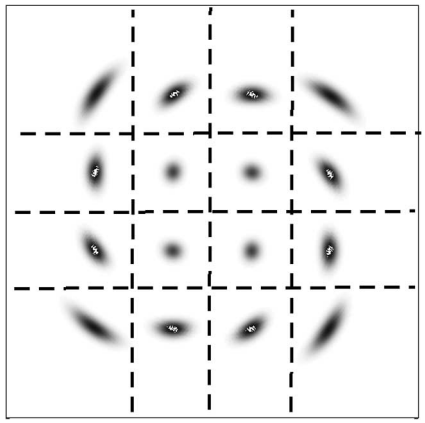

Fig. 10. Received signal pdf for a 16-QAM system with phase precompensation and NLPN postcompensation. (Dashed lines) Straight-line decision boundaries used for detection. The average power is -1 dBm, and the system length is 3000 km.

to mitigate phase noise such as those discussed in [8]–[10] and [14] may be beneficial. We focus on the technique studied by Ho and Kahn [14], which will be referred to as NLPN postcompensation. The phase of a received signal with power P_{rec} is rotated by an angle

$$\phi = -\gamma L P_{rec}/2 \tag{11}$$

according to Ho [2] and Liu *et al.* [15]. When phase precompensation is used with NLPN postcompensation, the resulting pdf is shown in Fig. 10 for $P_{avg} = -1$ dBm. In this case, the transmitted signal phase is not prerotated by $\overline{\theta_{NL}}$. Instead, the amount of prerotation is

$$\overline{\theta_{NL}} - E_P\left[\frac{\gamma L P_{rec}}{2}\right] = \overline{\theta_{NL}} - \frac{\gamma L(P+\sigma^2)}{2} \tag{12}$$

where $E_P[\cdot]$ denotes the expectation given a transmitted signal power P. The shape of the resulting pdf is less spiral-like and is closer to that of a linear 16-QAM system.

With these received signal pdfs, we implement the usual straight-line decision boundaries, which are shown as dashed

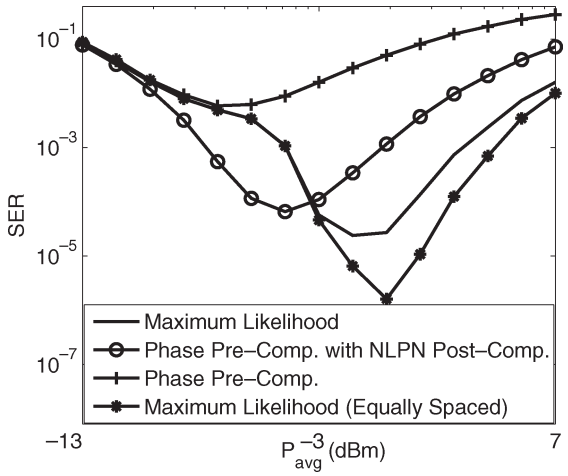

Fig. 11. SER as a function of average power for a square 16-QAM system using ML decision boundaries, phase precompensation with and without NLPN postcompensation, and straight-line decision boundaries. The system length is 3000 km.

lines in Figs. 9 and 10. The SERs of these schemes, together with the SER using the ML decision boundaries without phase precompensation and NLPN postcompensation, are shown in Fig. 11 for various input power levels. At low power levels, all three schemes similarly perform. This is in agreement with what was expected since NLPN is not dominant at low power levels, and the ML decision boundaries are close to a rectangular grid. Note that the performance using the ML decision boundaries is optimized at approximately $P_{rec} = -3$ dBm and degrades at high powers due to the increasing dominance of NLPN. Compared to the ML decision boundaries, the SER with phase precompensation is much higher. Phase precompensation with NLPN postcompensation significantly reduces the SER and even outperforms ML detection at low power levels. This is possible since after phase precompensation, the transmitted signal constellation set is different than the original square 16-QAM constellation, and hence, the SER is not necessarily lower bounded by that of a square constellation with its corresponding ML decision boundaries.

B. High Nonlinearity Regime

Fig. 12 shows the received pdf and the corresponding decision boundaries for the square 16-QAM constellation with $P_{avg} = 7$ dBm, which is a relatively high power. As shown in the figures, when the nonlinearity is high (large γ or high input power), the pdf and the decision boundaries are severely distorted by NLPN such that they bear little resemblance to those in a linear system. The shape of the pdf suggests that detection errors will be mainly caused by the received signal being incorrectly detected as a symbol having the same power but with a different phase than the correct one. Therefore, it might not be sensible to approximate ML detection with straight-line decision boundaries.

Fortunately, we can gain some insight into implementing ML detection when we look at the decision boundaries in a different way. Fig. 13 shows the same decision boundaries as Fig. 12 but in terms of r and θ. From the figure, we can see that the received

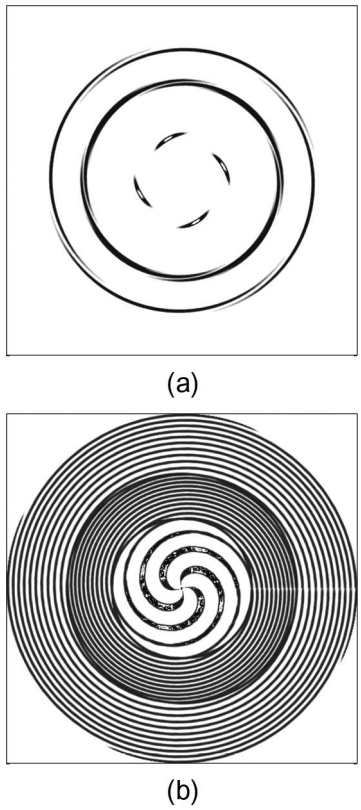

Fig. 12. (a) Received signal pdf and (b) corresponding ML decision boundaries for a 16-QAM system with $P_{avg} = 7$ dBm. The system length is 3000 km.

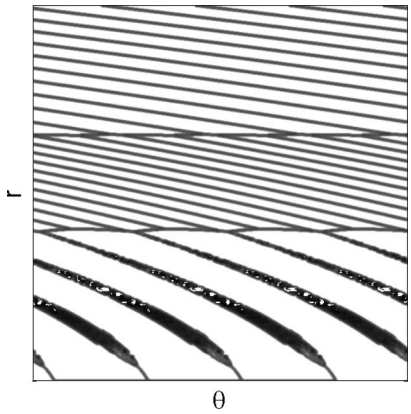

Fig. 13. ML decision boundaries for a square 16-QAM system with $P_{avg} = 7$ dBm in terms of r and θ. The system length is 3000 km.

signal can be mapped into three sets according to r independent of θ, corresponding to the three different input signal powers $\{P, 5P, 9P\}$ in the square 16-QAM constellation. The two values r_{15} and r_{59} that define the mapping are given by the intersections of the Rice pdfs

$$f_R(r_{15}, P) = f_R(r_{15}, 5P), \quad f_R(r_{59}, 5P) = f_R(r_{59}, 9P). \tag{13}$$

In this case, we can actually implement ML detection by first mapping the received signal to one of $\{P, 5P, 9P\}$ and then performing optimal phase postcompensation using the $\theta_c(r)$

corresponding to the mapped power. This mapping of r to $\{P, 5P, 9P\}$ is not error free since r is a noisy version of the input power; however, when such an error occurs, ML detection would have resulted in an error in the first place. Therefore, such a mapping-and-postcompensation strategy will not further degrade the system performance. After optimal phase postcompensation, the ML decision boundaries will be straight lines in terms of r and θ, and hence, the strategy outlined above is a practical way to approximate ML detection in 16-QAM systems with high nonlinearity. Furthermore, in a square 16-QAM constellation, since the phases of the signals with power $5P$ are not uniformly distributed, such a signal set may not be optimal in the high-nonlinearity regime, where phase noise is the performance-limiting factor. Consequently, a first step to optimize the signal set is to design the phase of these points to be equally spaced on $[0, 2\pi)$, and this signal set will be referred to as the *equally spaced set*. The resulting SER performance is shown in Fig. 11. As expected, the equally spaced set performs well when the power and, hence, nonlinearity are high and does not provide much of an advantage over the square 16-QAM constellation when the power is low and the system is essentially linear.

IV. Signal Constellation Optimization

In the previous section, we briefly studied signal point design to ease implementation of ML detection and improve SER performance for the case of 16-QAM systems with different degrees of nonlinearity. Ultimately, for a given γ, σ^2, number of signal points, and an average transmit power constraint, one might want to find the optimal signal constellation set that minimizes the SER. However, it is known that for non-Gaussian noise statistics, no analytical results for the optimal signal set exist [18], and numerical methods that are developed in solving such optimization problems are rather complicated [19]. Therefore, we only focus on four-point signal constellation optimization with some symmetry constraints such that the problem is more tractable, and the solution is more attractive for practical implementation purposes. Other than the 4-PSK modulation format, three constellation sets are considered: the 1–3 set with signal points located at $\{0, \sqrt{4P/3}, \sqrt{4P/3}e^{\pm j(2\pi/3)}\}$, the 2–2 set with points $\{\pm\sqrt{\varepsilon_1 P}e^{j\theta_1}\}, \sqrt{\varepsilon_2 P}e^{j(\pm(\pi/2)+\theta_2)}\}$, and the 1–2–1 set with points $\{0, \pm\sqrt{\epsilon_3 P}e^{j\theta_3}\}, \sqrt{\epsilon_4 P}e^{j(\pi/2+\theta_4)}\}$. These sets are shown in Fig. 14. The parameters ϵ_1, ϵ_2, and $\epsilon_3 < \epsilon_4$ are constrained such that the average power of each set is P, and θ_1, θ_2, θ_3, and θ_4 are determined by the phase precompensation technique described in the previous section.

Fig. 15 shows the SER using ML detection as a function of the average power for the various constellation sets considered with the ϵ parameters optimized for each average power. From the figure, we can see that as the average power goes up, a set with signal points having different power levels is preferred. This is due to the fact that NLPN increases with power, which results in the dominance of total phase noise over amplitude noise. In the limit that the impact of NLPN is severe, one can expect that a constellation set with all the signal points having different power levels (i.e., a 4-PAM constellation set) is optimal.

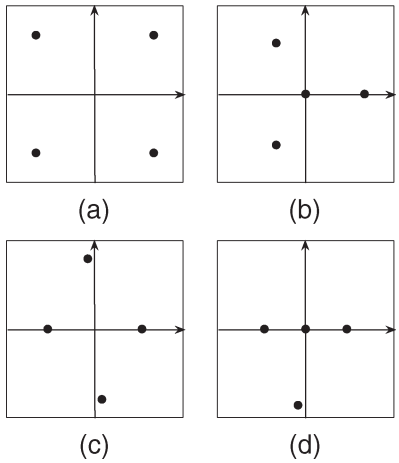

Fig. 14. Signal constellation sets studied for SER optimization. (a) 4-PSK set. (b) 1–3 set. (c) 2–2 set. (d) 1–2–1 set.

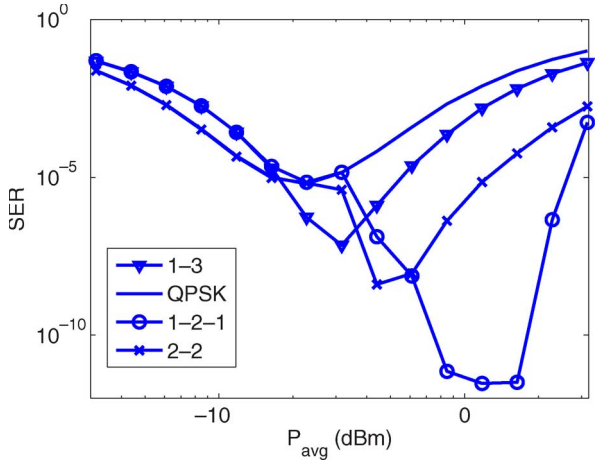

Fig. 15. SER for different four-point constellation sets as a function of average power. The system length is 7000 km.

V. Conclusion

In this paper, we studied signal design and implementation of ML detection for coherent optical transmission systems in the presence of linear phase noise and NLPN. We analytically derived the expression for the ML decision boundaries and the corresponding SER for M-ary PSK and DPSK systems with differentially coherent detection. The decision boundaries are in the form $\theta(r) = c_2 r^2 + c_1 r + c_0$, where θ and r are the phase and amplitude of the received signal, respectively. The impact of phase errors from synchronization on SER has also been investigated and was shown to be small for transoceanic links. For 16-QAM modulation formats, we studied various signal phase rotation techniques, including phase precompensation and NLPN postcompensation such that ML detection is well approximated by using straight-line decision boundaries. The problem of constellation set design for optimal SER performance was also considered for a system with four signal points. The impact of WDM effects and the interplay of chromatic dispersion and the Kerr effect on signal design and detection will be investigated in future work.

APPENDIX

A. Derivation of the Center Phase $\theta_c(r)$

The center phase satisfy (4)

$$f_{P,0}(r,\theta_c+\pi/M)=f_{P,0}(r,\theta_c-\pi/M).$$

Substitute (2) into (4), and after some algebraic manipulation

$$\sum_{m=1}^{\infty}|C_m(r)|\sin\Big(\frac{m\pi}{M}\Big)\sin[\arg\left(C_m(r)\right)+\ m\theta_c(r)]=0. \quad (14)$$

For high signal-to-noise ratio ($\rho_s \gg 1$), $x \ll 1$, and using the approximations $\sin\sqrt{jmx}\approx\sqrt{jmx}-(\sqrt{jmx})^3/3$, $\tan\sqrt{jmx}\approx\sqrt{jmx}+(\sqrt{jmx})^3/3$, and $I_m(y)\approx e^y/\sqrt{2\pi y}$ for large $|y|$

$$C_m(r)\approx 2r\left(1+\frac{jmx}{3}\right)e^{\rho_s jmx} \times e^{-\left[r^2+\rho_s(1+jmx)\right](1-jmx/3)}\frac{e^{2r\sqrt{\rho_s}\left(1+\frac{jmx}{3}\right)}}{\sqrt{4\pi r\sqrt{\rho_s}\left(1+\frac{jmx}{3}\right)}}$$

and the argument

$$\arg\left(C_m(r)\right)\approx\frac{mx}{3}\left(1+r^2+\rho_s+2r\sqrt{\rho_s}-\frac{1}{2}\right)$$

which is proportional to m. Therefore, if we write $\arg(C_m(r))\approx m\arg(C_1(r))$ and substitute back into (14)

$$\sum_{m=1}^{\infty}|C_m(r)|\sin\left(\frac{m\pi}{M}\right)\sin\left[m\left\{\arg\left(C_1(r)\right)+\theta_c(r)\right\}\right]=0$$

and the solution to the center phase will be given by

$$\begin{aligned}\theta_c(r)=&-\arg\left(C_1(r)\right)\\ =&\sqrt{\frac{x}{2}}\frac{\sin\sqrt{2x}-\sinh\sqrt{2x}}{\cosh\sqrt{2x}-\cos\sqrt{2x}}r^2\\ &-4\sqrt{\frac{\rho_s x}{2}}\frac{\sin\sqrt{\frac{x}{2}}\cosh\sqrt{\frac{x}{2}}-\cos\sqrt{\frac{x}{2}}\sinh\sqrt{\frac{x}{2}}}{\cosh\sqrt{2x}-\cos\sqrt{2x}}r\\ &+h(x,\rho_s)\end{aligned}$$

where

$$\begin{aligned}h(x,\rho_s)=&-\frac{\pi}{4}+\tan^{-1}\left(\cot\sqrt{\frac{x}{2}}\tanh\sqrt{\frac{x}{2}}\right)\\ &-\rho_s\sqrt{\frac{x}{2}}\frac{\sin\sqrt{2x}+\sinh\sqrt{2x}}{\cos\sqrt{2x}+\cosh\sqrt{2x}}\\ &+4\rho_s\sqrt{\frac{x}{2}}\frac{\sin\sqrt{2x}\cosh\sqrt{2x}-\cos\sqrt{2x}\sinh\sqrt{2x}}{\cosh 2\sqrt{2x}-\cos 2\sqrt{2x}}\end{aligned}$$

after some algebraic manipulations.

B. Derivation of the SER for Coherent Detection M-Ary PSK System

We need to evaluate the integral $\int_0^\infty|C_m(r)|dr$. Since $I_m(y)\approx e^y/\sqrt{2\pi y}$ for large $|y|$, we can write

$$|I_m(y)|\approx\mathbf{Re}\left\{I_m(y)e^{-j\mathbf{Im}\{y\}}e^{j\frac{1}{2}\arg(y)}\right\}.$$

Now, if we let

$$\begin{aligned}u_m(x)=&\left|\frac{\sec\sqrt{jmx}e^{\rho_s\sqrt{jmx}\tan\sqrt{jmx}}e^{-\frac{\alpha_m^2}{2s_m}}}{s_m}\right|\\ &\times e^{-j\frac{1}{2}\arg(\beta_m(x))}\\ \beta_m(x)=&\alpha_m/s_m\\ a_m(x)=&\mathbf{Re}\{1/2s_m\}\\ g_m(x)=&-\mathbf{Im}\left\{\beta_m(x)\right\}\end{aligned}$$

then the integral $\int_0^\infty|C_m(r)|dr$ is given by

$$\begin{aligned}&\mathbf{Re}\left\{u_m(x)\int_0^\infty re^{-a_m(x)r^2}e^{jg_m(x)r}I_m\left(\beta_m(x)r\right)dr\right\}\\ &=\mathbf{Re}\left\{u_m(x)\sum_{k=0}^{\infty}\int_0^\infty r\frac{(jg_m(x)r)^k}{k!}e^{-a_m(x)r^2}I_m(\beta_m(x)r)\right\}dr\\ &=\mathbf{Re}\left\{u_m(x)\sum_{k=0}^{\infty}\frac{(jg_m(x))^k}{k!}\right.\\ &\qquad\times\frac{\beta_m(x)^m\Gamma\left(\frac{m+k+2}{2}\right)}{2^{m+1}a_m(x)^{\frac{m+k+2}{2}}\Gamma(m+1)}\\ &\qquad\left.\times\ {}_1F_1\left(\frac{m+k+2}{2},m+1;\frac{\beta_m^2(x)}{4a_m(x)}\right)\right\}\end{aligned}$$

where the last two equalities follow from the Maclaurin series expansion of e^y and Gradshteyn and Ryzhik [20, Sec. 6.631]. The expression for SER then follows.

REFERENCES

[1] J. P. Gordon and L. F. Mollenauer, "Phase noise in photonic communications systems using linear amplifiers," *Opt. Lett.*, vol. 15, no. 23, pp. 1351–1353, Dec. 1990.

[2] K. P. Ho, *Phase-Modulated Optical Communication Systems*. New York: Springer-Verlag, 2005.

[3] W. T. Anderson *et al.*, "Modeling RZ-DPSK transmission—Simulations and measurements for an installed submarine system," presented at the Optical Fiber Commun. (OFC), Conf., Anaheim, CA, Mar. 2005, Paper OThC1.

[4] G. Charlet *et al.*, "Transmission of 40 Gb/s QPSK with coherent detection over ultra-long distance improved by nonlinearity mitigation," presented at the European Conf. Optical Commun. (fs), Cannes, France, Sep. 2006. Postdeadline paper.

[5] A. Mecozzi, "Long-distance transmission at zero dispersion: Combined effect of the Kerr nonlinearity and the noise of the in-line amplifiers," *J. Opt. Soc. Amer. B, Opt. Phys.*, vol. 11, no. 3, pp. 462–469, Mar. 1994.

[6] A. R. Charplyvy, "Limitations on lightwave communications imposed by optical-fiber nonlinearities," *J. Lightw. Technol.*, vol. 8, no. 10, pp. 1548–1557, Oct. 1990.

[7] A. Mecozzi, "On the optimization of the gain distribution of transmission lines with unequal amplifier spacing," *IEEE Photon. Technol. Lett.*, vol. 10, no. 7, pp. 1033–1035, Jul. 1998.
[8] A. P. T. Lau and J. M. Kahn, "Design of inline amplifier gains and spacings to minimize the phase noise in optical transmission systems," *J. Lightw. Technol.*, vol. 24, no. 3, pp. 1334–1341, Mar. 2006.
[9] A. P. T. Lau and J. M. Kahn, "Non-optimality of distributed amplification in presence of nonlinear phase noise," presented at the Optical Amplifiers Applications Coherent Optical Technologies Applications Conf., Vancouver, BC, Canada, Jun. 2006, Paper JWB23.
[10] A. P. T. Lau and J. M. Kahn, "Power profile optimization in phase-modulated systems in presence of nonlinear phase noise," *IEEE Photon. Technol. Lett.*, vol. 18, no. 23, pp. 2514–2516, Dec. 2006.
[11] S. K. Turitsyn, M. P. Fedoruk, V. K. Mezentsev, and E. G. Turitsyna, "Theory of optimal power budget in quasi-linear dispersion-managed fibre links," *Electron. Lett.*, vol. 39, no. 1, pp. 29–30, Jan. 2003.
[12] I. Nasieva, J. D. Ania-Castanon, and S. K. Turitsyn, "Nonlinearity management in fibre links with distributed amplification," *Electron. Lett.*, vol. 39, no. 11, pp. 856–857, May 2003.
[13] K.-P. Ho, "Mid-span compensation of nonlinear phase noise," *Opt. Commun.*, vol. 245, no. 1–6, pp. 391–398, Jan. 2005.
[14] K.-P. Ho and J. M. Kahn, "Detection technique to mitigate Kerr effect phase noise," *J. Lightw. Technol.*, vol. 22, no. 3, pp. 779–783, Mar. 2004.
[15] X. Liu *et al.*, "Improving transmission performance in differential phase-shift-keyed systems by use of lumped nonlinear phase-shift compensation," *Opt. Lett.*, vol. 27, no. 18, pp. 1616–1618, Sep. 2002.
[16] C. Xu and X. Liu, "Postnonlinearity compensation with data-driven phase modulators in phase-shift keying transmission," *Opt. Lett.*, vol. 27, no. 18, pp. 1619–1621, Sep. 2002.
[17] E. Ip and J. M. Kahn, "Feedforward carrier recovery for coherent optical communications," *J. Lightw. Technol.*, vol. 25, no. 9, pp. 2675–2692, Sep. 2007.
[18] D. H. Johnson and G. C. Orsak, "Relation of signal set choice to the performance of optimal non-Gaussian detectors," *IEEE Trans. Commun.*, vol. 41, no. 9, pp. 1319–1328, Sep. 1993.
[19] A. J. Kearsley, "Global and local optimization algorithms for optimal signal set design," *J. Res. Nat. Inst. Standards Technol.*, vol. 106, no. 2, pp. 441–454, Mar./Apr. 2001.
[20] I. S. Gradshteyn and I. M. Ryzhik, *Table of Integrals, Series, and Products*. New York: Academic, 1980.

Alan Pak Tao Lau (S'05) received the B.A.Sc. degree in engineering science (electrical option) and the M.A.Sc. degree in electrical and computer engineering from the University of Toronto, Toronto, ON, Canada, in 2003 and 2004, respectively. He is currently working toward the Ph.D. degree in electrical engineering at Stanford University, Stanford, CA.

His current interests include system-level designs of coherent optical fiber communication systems in the presence of nonlinearity.

Mr. Lau is the recipient of the National Science and Engineering Research Council Postgraduate Scholarship of Canada.

Joseph M. Kahn (M'90–SM'98–F'00) received the A.B., M.A., and Ph.D. degrees in physics from University of California, Berkeley, in 1981, 1983, and 1986, respectively.

From 1987 to 1990, he was with AT&T Bell Laboratories, Crawford Hill Laboratory, Holmdel, NJ. He demonstrated multigigabits-per-second coherent optical fiber transmission systems, setting world records for receiver sensitivity. From 1990 to 2003, he was with the faculty of the Department of Electrical Engineering and Computer Sciences, University of California, Berkeley, performing research on optical and wireless communications. From 1993 to 2000, he served as a Technical Editor for the *IEEE Personal Communications Magazine*. In 2000, he helped found StrataLight Communications, where he served as the Chief Scientist from 2000 to 2003. Since 2003, he has been a Professor of electrical engineering with Stanford University. His current research interests include single-mode and multimode optical fiber communications, free-space optical communications, and MEMS for optical communications.

Prof. Kahn received the National Science Foundation Presidential Young Investigator Award in 1991.